

Simulations of the effects of pre-seeded magnetic islands on the generation of runaway current during disruption on J-TEXT

Cite as: Phys. Plasmas **26**, 062508 (2019); <https://doi.org/10.1063/1.5100093>

Submitted: 15 April 2019 • Accepted: 21 May 2019 • Published Online: 19 June 2019

Z. H. Jiang, J. Huang,  R. H. Tong, et al.



View Online



Export Citation



CrossMark

ARTICLES YOU MAY BE INTERESTED IN

[Shattered pellet injection simulations with NIMROD](#)

Physics of Plasmas **26**, 042510 (2019); <https://doi.org/10.1063/1.5088814>

[First predictive simulations for deuterium shattered pellet injection in ASDEX Upgrade](#)

Physics of Plasmas **27**, 022510 (2020); <https://doi.org/10.1063/1.5133099>

[Theory of tokamak disruptions](#)

Physics of Plasmas **19**, 058101 (2012); <https://doi.org/10.1063/1.3703327>



Physics of Plasmas Physics of Fluids
Special Topic: Turbulence in Plasmas and Fluids
Submit Today!

Simulations of the effects of pre-seeded magnetic islands on the generation of runaway current during disruption on J-TEXT

Cite as: Phys. Plasmas **26**, 062508 (2019); doi: [10.1063/1.5100093](https://doi.org/10.1063/1.5100093)

Submitted: 15 April 2019 · Accepted: 21 May 2019 ·

Published Online: 19 June 2019





View Online



Export Citation



CrossMark

Z. H. Jiang,¹ J. Huang,¹ R. H. Tong,¹  T. T. Yang,¹ Z. F. Lin,¹ V. Izzo,²  C. H. Li,¹ Y. F. Liang,^{1,3,4,a)} X. Ye,¹ Y. H. Ding,¹ Z. Huang,¹ L. Z. Zhu,¹ and Z. Y. Chen^{1,5,b)}

AFFILIATIONS

¹International Joint Research Laboratory of Magnetic Confinement Fusion and Plasma Physics, State Key Laboratory of Advanced Electromagnetic Engineering and Technology, School of Electrical and Electronic Engineering, Huazhong University of Science and Technology, Wuhan 430074, China

²Fiat Lux, San Diego, California, USA and 9500 Gilman Dr., La Jolla, California 92093-0417, USA

³Institute of Plasma Physics, Chinese Academy of Sciences, Hefei 230031, China

⁴Forschungszentrum Jülich GmbH, Institut für Energie-und Klimaforschung-Plasmaphysik, 52425 Jülich, Germany

⁵Chengdu University, Chengdu 610106, China

^{a)}E-mail: y.liang@fz-juelich.de

^{b)}E-mail: zychen@hust.edu.cn

ABSTRACT

Simulations of argon (Ar) massive gas injection (MGI) into J-TEXT plasmas with 2/1 mode magnetic islands (mode penetration) are performed with the 3D magnetohydrodynamic (MHD) code NIMROD. In order to study the effect of the magnetic island phase on the loss of runaway electrons (REs) in disruption, four different phases of the pre-existing 2/1 magnetic island have been implemented. It is found that the RE confinement is drastically affected by the magnetic island phase during the thermal quench (TQ) phase. Simulation results show that the curve of the remaining RE ratio vs relative toroidal phase between the preseeded $m/n = 2/1$ islands and the MGI valve approximates a sinelike function dependence. The optimized phase difference for runaway suppression is predicted to be toroidal 90° ($\Delta\phi = \phi_{MGI} - \phi_{n=1}$). It is verified that the trajectories of low energy REs follow magnetic field lines strictly. A discrepancy in the evolution of the flux surface among different toroidal phases of 2/1 islands has been found, which greatly depends on the magnetic perturbations induced in disruption. A stronger low-order MHD activity might contribute to the accelerated processes of impurity assimilation and the TQ phase in the optimized phase. These simulations suggest that the relative phase between the MGI and 2/1 islands is important for RE suppression in future tokamaks.

Published under license by AIP Publishing. <https://doi.org/10.1063/1.5100093>

I. INTRODUCTION

Plasma disruption, which causes a localized heat flux to the divertor, a strong electromagnetic force on the plasma facing components (PFCs), and the generation of a large amount of high-energy runaway electrons (REs), is a critical safety problem for the reliable operation of the International Thermonuclear Experimental Reactor (ITER).^{1–5} Recently, the disruption induced by massive gas injection (MGI) of noble impurities has been studied extensively on a variety of tokamaks as a disruption mitigation scenario. Related experimental results have demonstrated the ability to radiate a large fraction of stored thermal and magnetic energies.⁶ However, due to a low impurity mixing efficiency in the plasma (only 25% of the Rosenbluth density), MGI prior

to the current quench (CQ) is estimated to be insufficient for completely suppressing the runaway electrons in the ITER disruptions.^{7–9} It is expected that approximately 70% of the predisruption plasma current (approximately 15 MA) can be converted to the RE current during disruptions in ITER. The disruption-induced REs may cause serious damage to the PFCs.^{2–5} Therefore, the ITER and future fusion reactors will need a reliable way to dissipate or suppress the RE current during the major plasma disruptions.^{10–14}

The suppression and the dissipation of the RE current have been investigated in several devices, such as JET, DIII-D, FTU, ASDEX Upgrade, and J-TEXT.^{2,15–18} In order to suppress the runaway current plateau, relevant experiments on MGI have been performed to

increase the electron density significantly.^{6,12,19,20} The enhancement of the electron density can produce larger drag force to overcome the force from the parallel electric field. In addition, the suppression of runaway current via increasing the magnetic perturbation has been reached.^{20–22} Intact nest magnetic surfaces can be destroyed to decouple the confinement of RE seeds due to a strong magnetic perturbation, which might avoid the occurrence of runaway avalanche. When the full suppression of runaway current cannot be achieved successfully, an alternative method of dissipation will be taken into account. The possibility of dissipating runaway current by MGI has been verified in several devices like DIII-D, JET, and J-TEXT.^{16–18} The massive injection of impurities can enhance both the drag and the synchrotron of REs, which has an important impact on the dissipation of REs. Nevertheless, it seems to be unreliable to fully suppress runaway current only by MGI since a poor gas mixing efficiency and extremely high density are required.

Accordingly, the application of resonant magnetic perturbation (RMP) to augment magnetic fluctuations has been proven to be a potential tool for suppressing REs.^{23–26} The formed stochastic magnetic surface can quickly expel RE seeds before they are amplified by the avalanche process.²² The experiments on TEXTOR have demonstrated that the runaway plateau can be suppressed by RMP during the MGI shutdown.²⁵ The significant suppression has already been reached by applying $n = 3$ mode RMP in DIII-D with a divertor configuration.²⁷ The RMPs with a dominant toroidal mode number of $n = 1$ have been used to significantly reduce runaway current during plasma disruption on the ASDEX Upgrade tokamak.¹⁵ However, the suppression of the generation of runaway current by RMP on the large machine JET did not work with a large distance between the RMP coils and target plasma. Several simulations have been performed to investigate the possibility of runaway suppression by RMP for the next generation machine ITER.^{28,29} It is found that REs will be rapidly lost if $\delta B/B \geq 10^{-3}$, which only corresponds to the region outside the normalized flux $\psi = 0.5$.²⁸ For large-scale machines, an alternative choice is to induce mode locking by RMP in plasma with magnetohydrodynamic (MHD) activities. In the J-TEXT tokamak, the effect of RMP on runaway suppression has been studied in the last few years. It has been demonstrated that a moderate amplitude 2/1 RMP can greatly reduce the runaway current plateau.³⁰ Additionally, the use of mode penetration induced by RMPs to suppress RE generation has also been achieved in J-TEXT.^{31,32} But the detailed physical mechanism of the effect of RMP on runaway suppression needs further investigation.

Many simulations have been performed to get a better understanding of the mechanism of runaway suppression.^{28,29,33,34} It is accepted that different magnetic perturbation configurations can determine the time dynamics and preferred loss directions of the REs regardless of particle energies and starting positions.²⁹ Besides, the effects of stochastic magnetic fields on RE confinement have already been explored in several theoretical^{35–40} and numerical^{28,29,34,41–43} studies. All these results reveal that a chaotic magnetic surface will be beneficial for RE loss. During the disruption, MHD activities are very strong and evolve rapidly. Therefore, it is important to simulate the results by considering the plasma responses, including the nonlinear evolution of MHD activities. Recently, the reduced MHD code, JOREK, has been applied to simulate MGI disruption mitigation and to investigate the mechanism of RE loss.^{44–46} The simulations show that the REs with different energies varying from 1 keV to 10 MeV

display a discrepant loss fraction during disruption.⁴⁶ As a pioneering study of RE dynamics during the disruption process, a test particle tracker was developed in NIMROD.^{47,48} The RE confinement for rapid shutdown scenarios in DIII-D, C-MOD, and ITER has been simulated with the NIMROD code, and an improved confinement in the limited shape is found due to both the spatial localization and the reduced toroidal spectrum in the nonlinear MHD activity. The RE confinement is also improved with the increasing device size.⁴⁷ Furthermore, disruption mitigation by MGI has been modeled for DIII-D plasmas with stationary, pre-existing islands. The results show that different phases of 2/1 islands can affect the parallel spreading of injected impurities.⁴⁹ The recent experiments scanning the toroidal phase of pre-existing 2/1 islands with a constant position of the MGI valve have been implemented on the J-TEXT tokamak. The experimental results show that the toroidal phase difference between the magnetic island and the MGI valve has a significant effect on plasma disruption. The thermal quench (TQ) duration is found to have a sinelike dependence on the toroidal phase difference,⁶¹ and different processes of disruption might also have an effect on runaway suppression. The experiments and simulations on J-TEXT also demonstrate that a full suppression can be reached by seeding large pre-existing 2/1 islands by mode penetration.³² But all the toroidal phase differences between the 2/1 magnetic island (“O” point) and the MGI valve in Ref. 32 are about 240° ($\Delta\phi = \phi_{MGI} - \phi_{n=1}$), which might not be the optimized phase for runaway suppression. So a comparatively large magnetic island might be required to fully suppress the runaway current plateau. But a large 2/1 island is not beneficial for the plasma stability. Thus, this paper will study the effect of different phases of pre-existing 2/1 islands on runaway suppression with the NIMROD code and try to make a prediction for experiment. In this work, the extended NIMROD includes options for the atomic/radiation physics associated with an impurity species and drift-orbit calculations for RE test particles (no feedback on the MHD fields).^{47,50} Importantly, the model also couples the plasma response of the RMP⁵¹ during the entire disruption process.

This paper is organized as follows. Section II describes the computational model used for the simulation. The numerical simulation results are presented in Sec. III. A significant effect of different phases of preseeded islands on RE loss is shown in Sec. III A. Section III B shows a discrepancy in the evolution of both field lines and magnetic perturbation between different phases of 2/1 islands. The complex MHD behaviors might be related to the impurity spreading and corresponding cooling. Finally, we discuss the conclusion in Sec. IV and summarize the simulation results in Sec. V.

II. COMPUTATIONAL MODEL

All the modeling results presented in this paper are performed with the extended NIMROD code.⁵² This code primarily evolves a set of nonlinear single-fluid MHD equations, including modified Faraday’s law, resistive MHD Ohm’s law, and Ampere’s law with the low-frequency limit, particle conservation, flow velocity evolution, and temperature evolution. Besides, a radiative cooling model KPRAD has been added to the extended code to simulate more realistic radiation rates during the rapid MGI-triggered shutdown process. Cooling due to ionization, radiation, and recombination is incorporated into the temperature evolution for a given impurity species, while the local Z_{eff} is incorporated into the Spitzer expression for resistivity.^{47,50}

Moreover, the guiding-center drift motion of the test REs can be calculated in this module as well.⁴⁷ The three-dimensional drift orbit calculation consists of three equations, including those pertaining to $\mathbf{E} \times \mathbf{B}$, curvature, and grad-B drifts, as follows:

$$dR = \frac{v_{\parallel} B_R}{B} dt + \frac{1}{B^2} [\mathbf{E} \times \mathbf{B}]_R dt, \quad (1)$$

$$dZ = \frac{v_{\parallel} B_Z}{B} dt + \frac{1}{R} \frac{\gamma m_e v_{\perp}^2}{2eB} dt + \frac{1}{R} \frac{\gamma m_e v_{\parallel}^2}{eB} dt + \frac{1}{B^2} [\mathbf{E} \times \mathbf{B}]_Z dt, \quad (2)$$

$$d\Phi = \frac{v_{\parallel} B_{\Phi}}{RB} dt + \frac{1}{RB^2} [\mathbf{E} \times \mathbf{B}]_{\Phi} dt. \quad (3)$$

Here, v_{\parallel} is the parallel velocity of REs along the magnetic field line (MFL); Runaway electrons can be accelerated by the parallel electric field and decelerated by collisions, synchrotron radiation, and bremsstrahlung radiation. The velocity component normal to the magnetic field is assumed based on a fixed pitch angle in the NIMROD code.⁴⁷ The constant pitch angle (v_{\perp}/v_{\parallel}) is estimated to be 0.1 according to J-TEXT experimental data, and a small error for the value of the pitch angle has a negligible effect on the final RE loss. For REs quickly accelerated to mega-electron-volt energies, the results are not highly sensitive to the starting energy of REs. Therefore, the energies of all the seed REs are initiated to be 150 keV and the test REs are initiated with random positions.

The perturbative field used in this work is produced by a set of dynamic RMP (DRMP) coils that are installed inside the vacuum chamber.⁵³ The DRMP coils can produce an $m/n = 2/1$ or $1/1$ dominated static or rotating magnetic perturbation. In our simulation, the DRMP coils are used to generate $m/n = 2/1$ dominated static magnetic perturbation. The magnetic field produced using DRMP coils is calculated based on the Biot-Savart law, and the results are regarded as a boundary condition in the NIMROD simulation. The amplitude of the $2/1$ magnetic field is about 10.4 Gs, and the current of DRMP coils is 4 kA.

All the simulations discussed in this paper begin from a kinetic EFIT (a equilibrium fitting code) reconstruction from J-TEXT. The pressure and q profiles for this equilibrium are shown in Fig. 1.

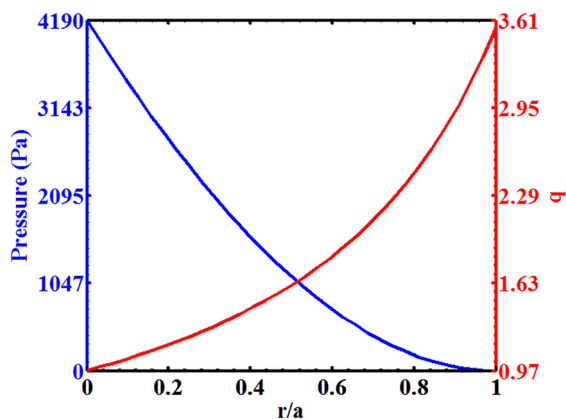


FIG. 1. Pressure and q profiles of the initial equilibrium.

III. COMPUTATIONAL RESULTS

A. Effect of the preseeded magnetic islands on RE confinement

Four rapid shutdown simulations with pre-existing $m/n = 2/1$ islands are performed in this work. The impurity gas of Ar is injected into the vacuum region with a prescribed spatial distribution first and then diffuses into the plasma area across the last closed flux surface (LCFS) to trigger the plasma disruption. The initial distribution of Ar impurities is shown as the color contours in Figs. 2(a) and 2(b). An MGI valve is setup at a poloidal angle of -90° and a toroidal angle of 0° as the yellow contour regions show. The last closed flux surface is plotted as the solid green circle. The impurity gas is continuously injected from $t = 0.05$ ms to $t = 0.15$ ms at a constant rate.

Before MGI, $2/1$ islands with a specified phase excited by RMP have already been seeded in the plasma area. The RMP is powered at $t = 0$ ms, and the current of RMP coils reaches 4 kA at $t = 0.02$ ms with a rapid increase during this duration. The mode penetration can occur, and there is an onset of $m/n = 2/1$ islands at $t = 0.05$ ms. Four different phases of $2/1$ islands are shown in Fig. 2. The Poincare plots of the field lines at a toroidal angle of 0° at $t = 0.06$ ms are shown in Figs. 2(a)–2(d). Red circles and x points are marked to indicate the o-points and x-points of $2/1$ islands. It is found that the difference in the poloidal degree of the O point of $2/1$ islands between (a) and (b) is about 90° . The same difference value can also be found between (c) and (d). Taking the MGI valve as the reference angle, Fig. 2(e) shows the amplitudes of poloidal magnetic field B_θ for these four cases vs toroidal angle after mode penetration. It is observed that there is an $n = 1$ mode perturbation in B_θ that can be used to indicate the toroidal phase of $2/1$ islands. The black circle, green triangle, red +, and blue star correspond to (a), (b), (c), and (d), respectively, and their toroidal phases of the O point of $2/1$ islands are 120° , 300° , 45° , and 225° in sequence. The toroidal phase difference between (a) and (b) is 180° , and that between (c) and (d) is also the same.

A process of shutdown will begin shortly after MGI for these four cases. Taking case toroidal 45° as an example, Fig. 3 shows a typical time trace of the core temperature (near the magnetic axis), plasma current, and kinetic energy of REs initially at different radial positions from $t = 0$ to $t = 1.2$ ms. These three evolutions only include the TQ phase but not the CQ phase as primary RE loss occurs in the TQ phase. The more detailed discussion about the TQ duration is shown later. The core temperature of plasma begins to decrease near $t = 0.94$ ms as shown in Fig. 3(a), and the CQ begins near $t = 1.05$ ms at the moment of the maximum peak of plasma current as shown in Fig. 3(b). There are two times of rapid ascent of plasma current near $t = 0.94$ ms and $t = 0.98$ ms successively, resulting in two peaks of plasma current, and the second peak is larger. In the TQ phase, a rapid increase in plasma current is commonly attributed to the occurrence of an internal reconnection event which tends to flatten the current profile (and reduce internal inductance l_i) since that poloidal flux ($l_i I_p$) cannot change instantaneously.^{36,54} So two times strong internal reconnection event at these two moments might exist, and the second is stronger. Similar events also occur in other three cases during the disruption phase. But different toroidal phases might affect the start and end time of TQ, which will eventually result in different TQ durations. Typically, the TQ duration for toroidal 45° is 0.18 ms, but that for toroidal 225° is 0.145 ms. More details will be described later.

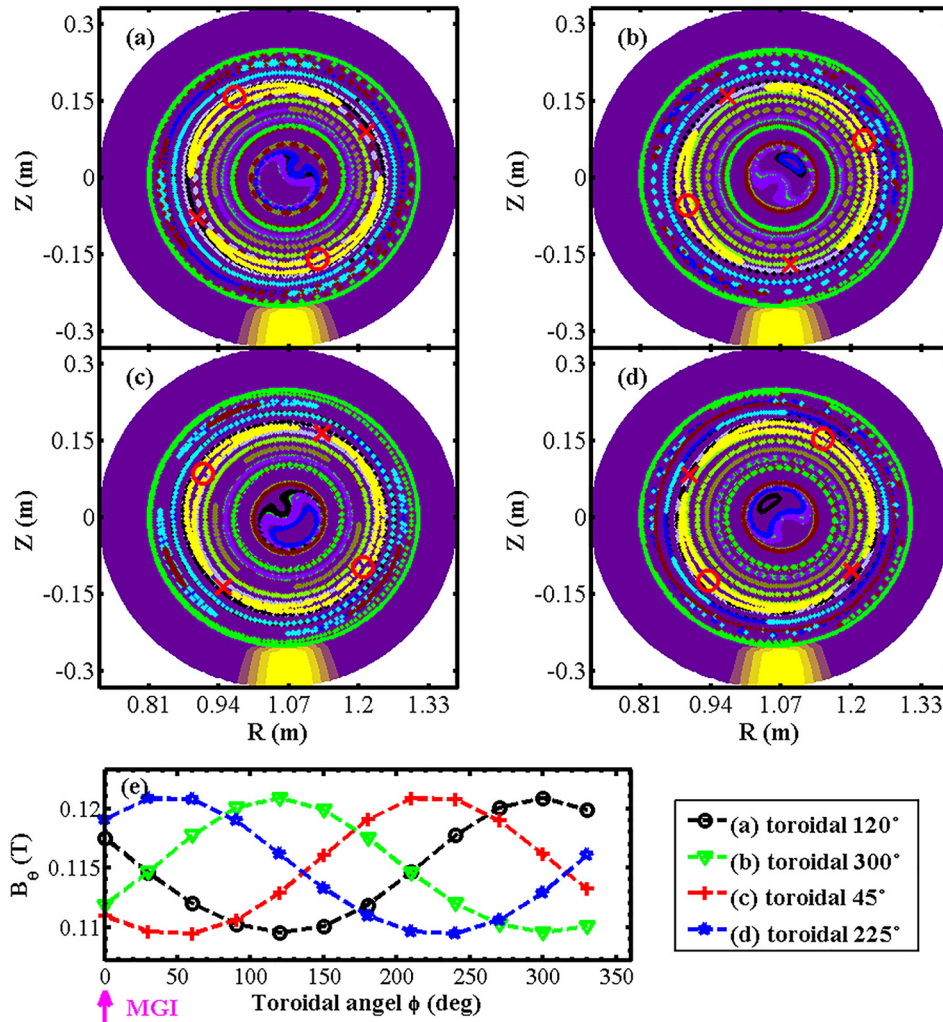


FIG. 2. (a)–(d) Poincaré plots of the field lines at a toroidal angle of 0° superimposed on color contours of the MGI source distribution at $t = 0.06$ ms. An MGI valve is setup at a poloidal angle of -90° and a toroidal angle of 0° as the yellow contour regions show. Red “o” and “x” points are marked to indicate the o-points and x-points of $m/n = 2/1$ islands. The last closed flux surface is plotted as the solid green circle. Both the plasma current (I_p) and the toroidal field (B_t) are perpendicular to the paper facing outward. (e) The amplitude of B_θ after mode penetration vs the toroidal angle. The black circle, green triangle, red “+,” and blue star correspond to (a), (b), (c), and (d), respectively, and their toroidal phases are 120° , 300° , 45° , and 225° in sequence. The toroidal phase difference between case (a) and case (b) is 180° , and that between case (c) and case (d) is also the same value.

The REs' kinetic energy evolution with three different initial locations is shown in Fig. 3(c). The red line, blue line, and green line correspond to some REs near the edge, the location of $q = 2$, and the core of plasma, respectively. The kinetic energy of REs will become zero when they hit the device. It is noted that the REs near the edge of plasma first hit the device wall (before TQ) and the other one near the $q = 2$ surface escapes more slowly (near the TQ), but the REs in the core are confined well. Besides, the REs near the edge are accelerated first, whereas the REs in the core last, because the high Z_{eff} and corresponding cooling induced by the impurity spreading appear at the edge at first, which will induce a large parallel electric field to accelerate REs.⁴⁷ The related theory of RE acceleration has been discussed in Ref. 45. The kinetic energy of the RE near the core can be accelerated into a high value in a short time. In the simulation, the maximum induced parallel electrical fields for toroidal 45° and toroidal 225° are 100 V/m and 150 V/m, respectively. These three kinds of REs only represent the characteristics of REs initially at different radial positions during disruption, and the inner REs are more difficult to escape than the outer regime.

During the TQ duration, a significant effect of initial toroidal phases of $2/1$ islands on RE loss is shown in Fig. 4. In this paper, a fraction of confined electrons is defined as the ratio that the number of confined REs accounts for the number of all initial REs ($N_{confined}/N_{initial}$). The remaining RE ratio is calculated by dividing the number of remaining REs after the TQ by the number of all initial REs ($N_{remaining}/N_{initial}$). Figure 4(a) shows detailed time traces of the evolution of the fraction of confined REs for these four cases. All the fractions before $t = 0.9$ ms are similar, and they begin to rapidly decrease shortly after TQ (after $t = 0.9$ ms). The fraction for each case experiences two rapid crashes during a TQ duration, and a weak plateau between the two crashes is formed. For example, the two events for case toroidal 45° occur near $t = 0.94$ ms and $t = 0.98$ ms, respectively, but it is near $t = 0.96$ ms and $t = 1.01$ ms when these two crashes occur for case toroidal 225° . So the first rapid loss of REs begins shortly after the start of TQ and the second is near the beginning of CQ. What is more, the crash for case toroidal 225° is more rapid than that for case toroidal 45° . The same result is also obtained between case toroidal 120° and case toroidal 300° .

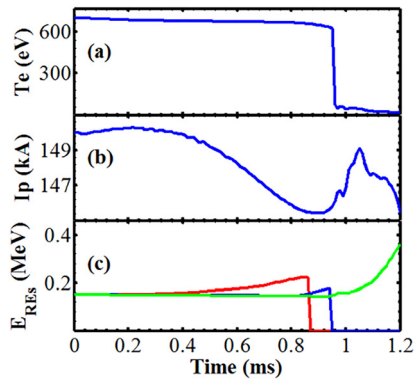


FIG. 3. A time trace of core temperature, plasma current, and the evolution of RE energy during the rapid shutdown for case toroidal 45° : (a) T_e (electronvolts), the electron temperature in the core of the plasma. (b) I_p (kiloampere), the current of the plasma. (c) E_{REs} (mega-electron-volt), the kinetic energy of the REs initially at different radial positions. The red line, blue line, and green line correspond to some REs near the edge, around $q=2$, and at the core of plasma, respectively.

After $t = 1.1$ ms (in the CQ stage), the remaining REs are confined very well and formed the RE plateau. The dependence of the remaining RE ratio after the TQ on the toroidal phase of 2/1 islands is shown in Fig. 4(b). The ratio of REs for case toroidal 225° is the lowest, whereas the ratio with a reverse phase such as case toroidal 45° is the highest. Considering the effect of applied $n=1$ magnetic perturbation on remaining REs, the dependence relationship is fitted by a sinelike function. The results suggest an optimized toroidal phase of 2/1 islands which is beneficial for RE loss that might exist in the J-TEXT, and the phase is predicted to be about toroidal 270° according to the $n=1$ fitting function. So the optimized toroidal phase difference between the 2/1 magnetic island and the MGI valve is predicted to be about 270° or 90° .

B. Stochastic magnetic surface and MHD activity

A discrepancy of RE confinement among these four cases during disruption has been presented, and the dependence of the remaining RE ratio on the relative toroidal phase between 2/1 islands and the MGI valve is also found in Sec. III A.

The trajectories of low-energy REs depend significantly on the trails of the magnetic field lines (MFLs).⁴² Thus, the degree of stochasticity of the magnetic surface can indicate RE confinement.^{36,46} The evolution of the magnetic surface for case toroidal 45° and toroidal 225° is shown in Fig. 5. Few intact magnetic surfaces survive during the TQ duration as shown in (a) and (c) because of a complex MHD activity. But a comparable difference existing in the CQ phase can be seen as shown in Figs. 5(b) and 5(d). It is observed that the magnetic surface recovers faster for toroidal 45° than toroidal 225° because toroidal 45° features more intact nest magnetic surfaces than toroidal 225° in the core of plasma at $t = 1.52$ ms.

What is more, there will be a large amount of open MFLs that directly connect into the device wall after finite toroidal turns during plasma disruption. These open MFLs play a vital role in expelling most REs from the plasma core regime. However, the numbers of toroidal turns of whirling for open MFLs before touching the device wall display a difference between case toroidal 45° and toroidal 225° . In this paper, the length of open MFL from the starting selected point

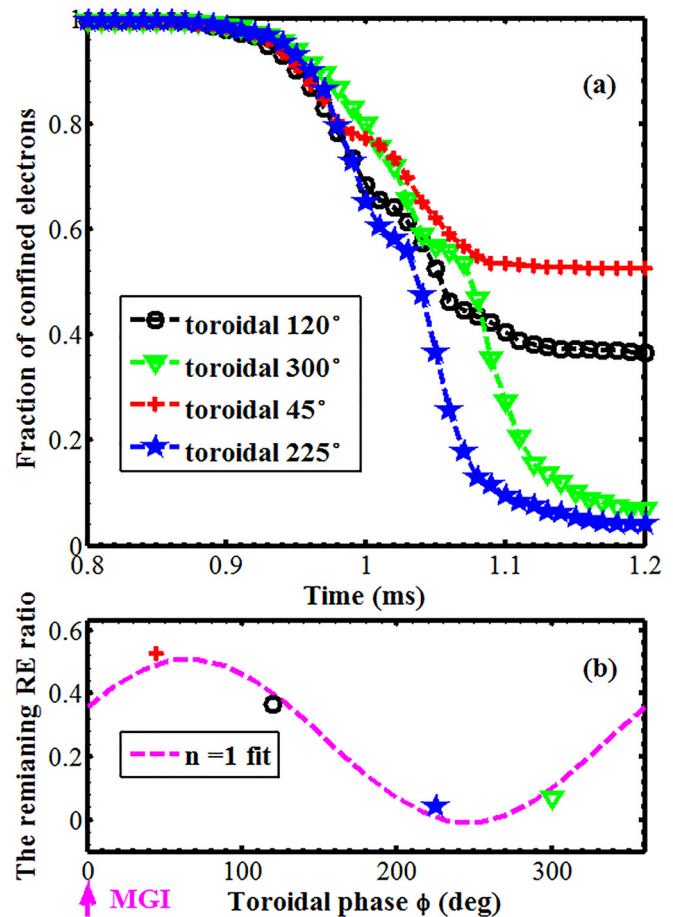


FIG. 4. The effect of different phases of pre-existing 2/1 islands on RE loss. (a) Fraction of confined REs vs time (millisecond) for four cases. The black circle, green triangle, red +, and blue star correspond to a toroidal phase of 120° , 300° , 45° , and 225° of 2/1 islands, respectively. (b) The dependence of the remaining RE ratio after the TQ on the toroidal phase of 2/1 islands. The relationship between the remaining ratio of REs and the toroidal phase approximately a sine like dependence.

to the device wall is defined as the connection length of MFL. The connection length of closed MFL is theoretically infinite. But a finite number of the most turns of 200 are set in NIMROD numerical simulation, and the maximum connection length of open MFL is approximate 1200 m (the major radial of J-TEXT is 1.05 m). In this work, all MFLs are classified into three classes according to their lengths as Fig. 6 shows: short MFLs (blue points) range from 0 to 200 m; intermediate-length MFLs (red points) range from 200 to 1100 m; and long MFLs (green points) range from 1100 to 1300 m. A first observation in Fig. 6 is that the number of short or intermediate-length MFLs for case toroidal 45° [Fig. 6(a)] is significantly less than that for toroidal 225° [Fig. 6(b)] at $t = 1.05$ ms. The blue points for toroidal 225° are almost fully distributed at the high-field side and the low-field side, whereas those for toroidal 45° are only partial at the low-field side.

To illustrate the relationship between MFLs and RE confinement more clearly, a fraction of short MFLs (the normalized number of short MFLs at every moment) and RE loss (the loss rate of REs at every

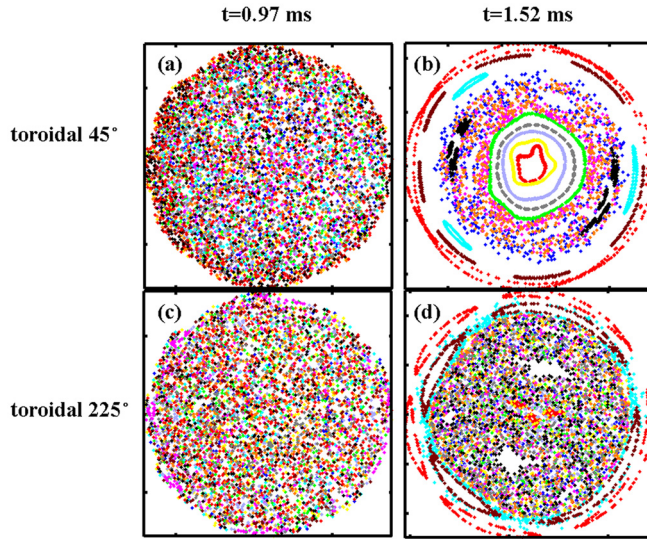


FIG. 5. Poincare plots for cases toroidal 45° and toroidal 225° at $t = 0.97$ ms (in the TQ phase) and $t = 1.52$ ms (in the CQ phase), respectively. (a) $t = 0.97$ ms for toroidal 45°, (b) $t = 1.52$ ms for toroidal 45°, (c) $t = 0.97$ ms for toroidal 225°, and (d) $t = 1.52$ ms for toroidal 225°.

moment) are calculated. The overall time traces of both these quantities for case toroidal 45° and toroidal 225° are shown in Fig. 7. The RE loss and the fraction of short MFLs for the two cases have nearly the same evolution shape from 0.8 ms to 1.2 ms. Before $t = 0.9$ ms, only a few REs are lost. Most of these lost REs are initially at the edge of plasma as a small fraction of short MFLs appear in the same region. The fraction of short MFLs begins to remarkably increase shortly after TQ due to a stronger stochasticity in the core, and so a conspicuous increase in RE loss throughout the area begins. Moreover, two distinct peaks of the fraction of short MFLs with the two corresponding peak values of RE loss are seen in each of the two cases. The first peak is near the start of TQ, and the second is near the beginning of CQ. After the second peak, both the fraction of short MFLs and RE loss begin to decrease for the two cases. It is noted that the fraction of short MFLs

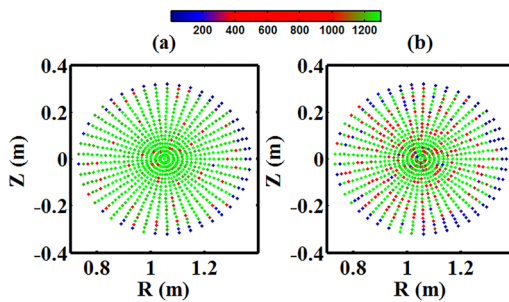


FIG. 6. Poloidal scatter plots of the connection length of MFL at a toroidal angle of 0° at $t = 1.05$ ms. (a) Toroidal 45° and (b) toroidal 225°. The color bar represents different values of the length. All the MFLs are classified into three classes according to their connection lengths: short MFLs (blue points) range from 0 to 200 m; intermediate-length MFLs (red points) range from 200 to 1100 m; and long MFLs (green points) range from 1100 to 1300 m.

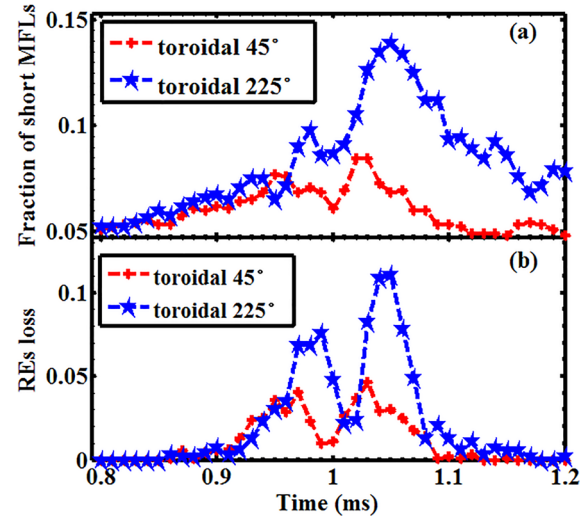


FIG. 7. Time traces of two quantities for case toroidal 45° and toroidal 225° (from 0.8 ms to 1.2 ms): (a) fraction of short MFL. (b) RE loss. Here, the fraction of short MFL refers to the normalized number of short MFLs at every moment. RE loss refers to the loss rate of REs at every moment.

for toroidal 225° is always higher than that for toroidal 45°, which leads to a higher loss rate of REs for the former phase.

The result demonstrates that the RE loss and the fraction of short MFLs have very strong correlations, confirming that the escape of low-energy REs primarily follows the trails of short MFLs. The variation of the fraction of short MFLs over time originates from complex MHD activity during the TQ duration. The magnetic perturbation (calculated from the formula $\delta B/B \approx \sqrt{W_{mag,n}/W_{mag,0}}$ ⁵⁵) from $n = 1$ to $n = 3$ toroidal components is calculated for toroidal $\phi = 45^\circ$ and toroidal $\phi = 225^\circ$ as shown in Fig. 8. The $n = 0$ mode perturbation for the two cases is identical, and all amplitudes of magnetic perturbations from the $n = 1$ to $n = 5$ component before $t = 0.8$ ms are also identical. But almost every component from $n = 1$ to $n = 5$ for toroidal 225° is larger than that for toroidal 45° in the disruption. In addition, the $n = 1$ component for both phases is larger than other n mode components. In each of the two phases, there are two times of ascent of $n = 1$ mode perturbation resulting in two peaks during plasma disruption. The first peaks of $n = 1$ perturbation marked by two vertical thin black lines are near the start time of TQ, and the second peaks marked by two vertical thin green lines are near the CQ. The two peaks for toroidal 225° are larger than those for toroidal 45°.

Therefore, a stronger MHD activity is implied in the disruption for case toroidal 225°. The complex MHD activity might be related to impurity spreading and corresponding cooling. The amount of ionized Ar inside three different magnetic surfaces is shown in Fig. 9, and the contours of the temperature profile toroidally and poloidally averaged are presented in Fig. 10. The amount of Ar outside $q = 2$ means the amount of Ar between $q = 2$ and LCFS. The TQ start is signaled when the cooling around $q = 2$ ($R = 1.2$ m) begins to accelerate. It is found that the amount of Ar deposited inside $q = 2$ for toroidal 225° is more than that for toroidal 45° throughout the disruption phase as shown in Fig. 9(a). Additionally, the increase in the amount of Ar inside $q = 2$ is more sharp for toroidal 225° in the TQ phase. Accordingly, the TQ

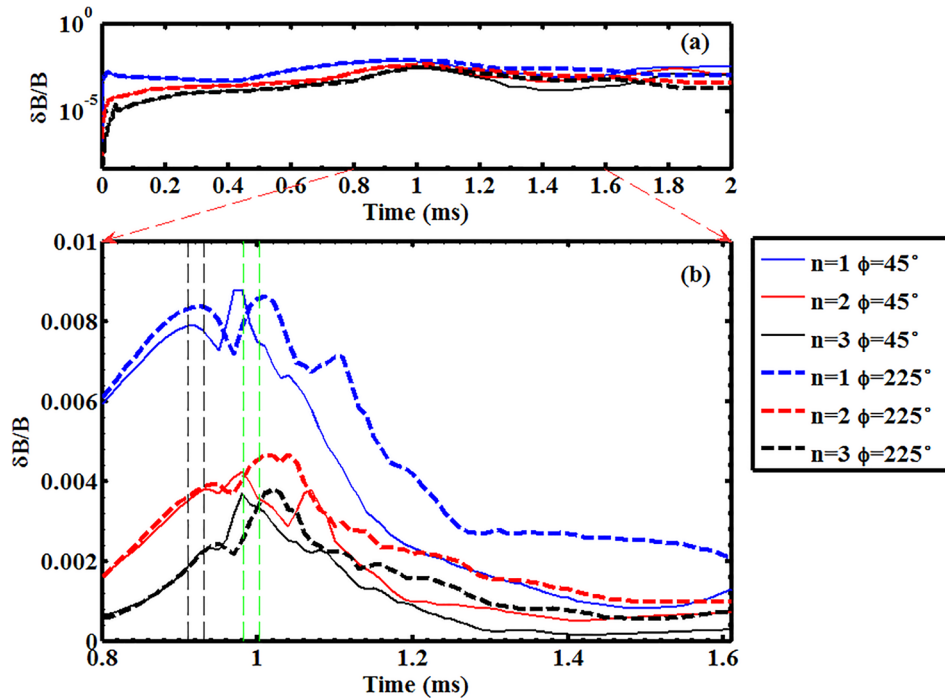


FIG. 8. Magnetic perturbations ($\delta B/B$) from $n=1$ to $n=3$ toroidal components (the amplitude of the $n=0$ mode is 1, and it is considered as a reference): (a) the process including the $n=1$ to $n=3$ toroidal components from $t=0$ ms to $t=2$ ms; (b) a partial process including from $t=0.8$ ms to $t=1.6$ ms. The solid and dashed curves represent toroidal 45° ($\phi = 45^\circ$) and toroidal 225° ($\phi = 225^\circ$), respectively. The two vertical thin black lines indicate the first peak of $\delta B/B$, and the two vertical thin green lines indicate the second peak of $\delta B/B$.

duration is shorter for case toroidal 225° than toroidal 45° as shown in Fig. 10. The results reveal that impurity spreading might be affected by the phase of 2/1 islands to some extent, and an appropriate phase might promote the diffusion of impurities into the $q=2$ surface and accelerate the TQ phase. Nonetheless, the amount of Ar outside $q=2$ for the former is less than the latter, which result in a little more amount of Ar outside LCFS for toroidal 45° . The phenomenon might be related to the impurity spreading across LCFS. The impurities that diffuse into the $q=2$ surface and the extent of the corresponding cooling can lead to a shrinkage of current density. The missing current might cause the appearance of magnetic islands, and the same current perturbation would also cause a magnetic perturbation δB .⁵⁶ The effectiveness of gas-jet penetration to various depths, and the corresponding destabilization has been investigated in Ref. 57.

IV. DISCUSSION

The effect of the relative toroidal phase between pre-existing 2/1 islands and the MGI valve on the runaway suppression is investigated in this paper. The simulation results show that a sinusoidal dependence of the remaining RE ratio on the toroidal phase of islands might exist on the J-TEXT tokamak when the location of the MGI valve is constant. The most appropriate phase to suppress runaway current is predicted to be toroidal 270° . Nevertheless, not only the phase but also the width of pre-existing 2/1 islands has a significant effect on RE suppression. The 2/1 islands excited in this work are not very large with a short duration of mode penetration. The experiments and simulation on J-TEXT have demonstrated that a full runaway suppression can be reached by implementing a large magnetic island before MGI.³² Unlike small islands, a larger island will directly induce strong magnetic fluctuation before MGI and a stronger magnetic perturbation during the disruption phase, which results in an enhancement of the

loss of RE seeds and fully suppresses runaway current as shown in Figs. 6 and 10 in Ref. 32. But on the other hand, the larger 2/1 magnetic island can also cause a disruption in advance.⁴⁹ Therefore, a properly large island with an appropriate phase might be most beneficial for both runaway suppression and plasma stability.

Recent J-TEXT disruption experiments with toroidal phase scanning of pre-existing 2/1 islands have been performed, and the effect of 2/1 islands on the disruption process on J-TEXT has been presented in Ref. 61. A distinct sinelike dependence of the TQ duration on the toroidal phase of the $n=1$ mode is shown in a figure in Ref. 61. It is found that the TQ duration is shortest when the relative toroidal phase between the $n=1$ mode and the MGI valve is toroidal 90° ($\Delta\phi = \phi_{MGI} - \phi_{n=1}$). But more precise conclusion for runaway suppression still requires more experiments to investigate. A similar experimental result that an appropriate phase of upper-to-lower B-coil might result in a significantly reduced current and lifetime of the generated RE beam in plasma disruption has been presented.¹⁵

The effect of pre-existing islands on RE loss is determined by the degree of stochasticity of the magnetic surface in MGI shutdown. During disruption, a comparatively complex MHD activity and a large magnetic perturbation are induced, which will cause chaotic magnetic surfaces. In the simulation, the complex MHD activity might be related to impurity spreading and the corresponding cooling, and an accelerated process in both the diffusion of impurities and the TQ phase is seen. The discrepancy of impurity diffusion occurs around $q=2$, which reveals an effect of 2/1 islands on impurity spreading. But the mechanism that the 2/1 islands affect impurity spreading is not studied in this paper. The impurity spreading might be related to various factors such as the particle transport by $E \times B$ convection⁵¹ and formation of multiple branches of impurity plume due to the growth of the higher n modes.⁴⁹ The detailed physical mechanism needs

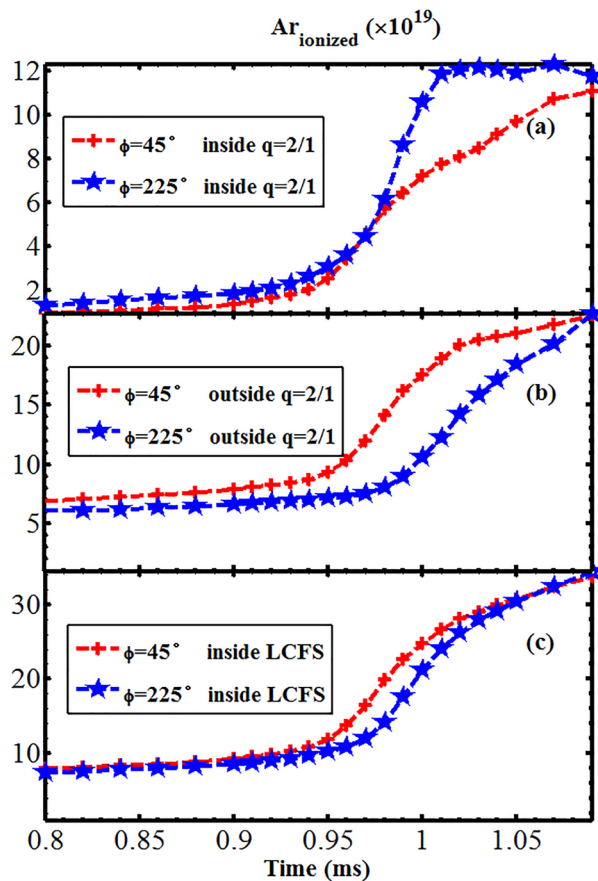


FIG. 9. The amount of ionized argon inside different magnetic surfaces vs time (millisecond). (a) Inside $q = 2$, (b) outside $q = 2$, and (c) inside LCFS. The amount of Ar outside $q = 2$ means the amount of Ar between $q = 2/1$ and LCFS.

further investigation in the future. Nonetheless, the used RMP in this work also contains small $m = 3$ and $m = 1$ mode components. So a small $1/1$ and $3/1$ islands might also be excited in the plasma, which might have a little effect on impurity spreading and corresponding MHD activity as the width of these islands is small. The effect caused by $1/1$ and $3/1$ islands will be studied in our future work. Moreover, the population of all initial REs in these cases is the same, and there is no calculation of primary and hot tail RE generation in the NIMROD model. But in real experiments, the generation of REs during the TQ phase might be affected by the evolution of electron temperature, the electric field, and the density of plasma.⁵⁸ Some other theoretical results also show that RE generation can be affected by the resultant density because of different impurity contents⁵⁹ and radial diffusion loss caused by stochastic magnetic perturbation.³⁸ In our simulations, it is shown that there is a discrepancy in the evolution in T_e , the impurity assimilation, and MHD activity, which might affect RE generation in a way. A shorter TQ duration due to an increased impurity assimilation might be beneficial for RE generation from the hot tail.⁶⁰ But the critical electric fields for sustainment of the existing REs might also be increased due to a stronger stochasticity and MHD activity as shown in Ref. 38. Meanwhile, the mechanism of the secondary

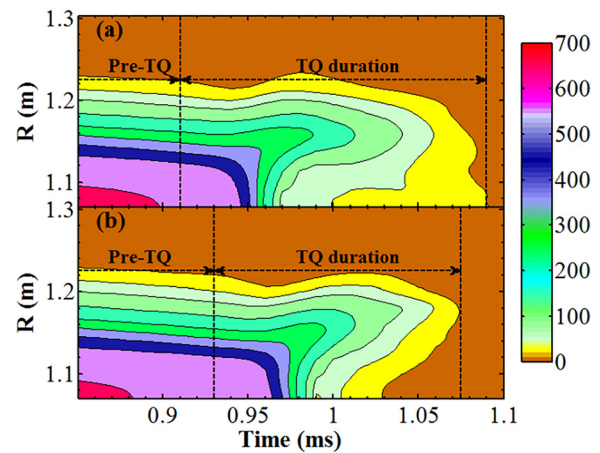


FIG. 10. Contours of the profile of temperature, toroidally and poloidally averaged vs time, and major radius (R) for (a) toroidal 45° and (b) toroidal 225° . Vertical dashed black lines indicate the start and end times of the TQ phase.

generation of RE due to avalanche is not incorporated, which does not match experiments very well. But the runaway current plateau on J-TEXT can also be predicted approximately according to expression (1) in Ref. 48.

V. SUMMARY

Simulations of MGI shutdown triggered by Ar impurities with the pre-existing $2/1$ islands have been performed with the NIMROD code. During plasma disruption, the RE confinement in four cases with different phases of $2/1$ islands is investigated. The results show that the curve of the remaining RE ratio vs relative toroidal phase between $2/1$ islands and the MGI valve approximates a sinelike dependence. The optimized phase difference between $2/1$ islands and the MGI valve for suppressing runaway current is predicted to be about toroidal 90° (270°). More precise conclusion for runaway suppression still requires more experiments to certify. The numerical results show that the trajectories of low-energy REs are determined by the degree of stochasticity of the magnetic surface in MGI shutdown. The magnetic topology structure greatly depends on the magnetic perturbation that is induced by complex MHD activity during plasma disruption. These MHD activities might be related to the process of impurity spreading and the corresponding cooling, and an appropriate phase of pre-existing $2/1$ islands might accelerate the diffusion of impurities across the $q = 2$ surface and result in a faster process of the TQ phase. These simulations suggest that the relative toroidal phase between the MGI valve and the pre-existing $2/1$ islands is important for runaway suppression on J-TEXT tokamaks, which might give some insights into future tokamaks.

ACKNOWLEDGMENTS

The authors are very grateful for the help from the J-TEXT team and the NIMROD team. This work was partially supported by the National Magnetic Confinement Fusion Science Program (Nos. 2015GB111002 and 2015GB104004), the National Natural Science Foundation of China (Nos. 11575068 and 11775089), and the National Key Research and Development Program of China (Nos. 2017YFE0300500 and 2017YFE0300501).

REFERENCES

- ¹V. Riccardo, "Disruptions and disruption mitigation," *J. Plasma Phys. Controlled Fusion* **45**(12A), A269 (2003).
- ²N. Commaux, L. R. Baylor, T. C. Jernigan, E. M. Hollmann, P. B. Parks, D. A. Humphreys, J. C. Wesley, and J. H. Yu, "Demonstration of rapid shutdown using large shattered deuterium pellet injection in DIII-D," *Nucl. Fusion* **50**(11), 112001 (2010).
- ³S. Putvinski, P. Barabaschi, N. Fujisawa, N. Putvinskaya, M. Rosenbluth, and J. Wesley, "Halo current, runaway electrons and disruption mitigation in ITER," *J. Plasma Phys. Controlled Fusion* **39**(12B), B157 (1997).
- ⁴F. Schuller, "Disruptions in tokamaks," *J. Plasma Phys. Controlled Fusion* **37**(11A), A135 (1995).
- ⁵T. C. Hender, J. C. Wesley, J. Bialek, A. Bondeson, A. H. Boozer, R. J. Buttery, A. Garofalo, T. P. Goodman, R. S. Granetz, Y. Gribov *et al.*, "Chapter 3: MHD stability, operational limits and disruptions," *Nucl. Fusion* **47**(6), S128–S202 (2007).
- ⁶G. Pautasso, C. J. Fuchs, O. Gruber, C. F. Maggi, M. Maraschek, T. Pütterich, V. Rohde, C. Wittmann, E. Wolfrum, P. Cierpka *et al.*, "Plasma shut-down with fast impurity puff on ASDEX Upgrade," *Nucl. Fusion* **47**(8), 900–913 (2007).
- ⁷M. Lehnen, A. Alonso, G. Arnoux, S. Bozhnikov, S. Brezinsek, T. Eich, K. Finken, A. Huber, S. Jachmich, and U. Kruezi, "First experiments on massive gas injection at JET—consequences for disruption mitigation in JET and ITER," in *Proceedings of the 36th EPS Conference on Plasma Physics Sofia* (Bulgaria, 2009).
- ⁸E. M. Hollmann, P. B. Aleynikov, T. Fülöp, D. A. Humphreys, V. A. Izzo, M. Lehnen, V. E. Lukash, G. Papp, G. Pautasso, F. Saint-Laurent *et al.*, "Status of research toward the ITER disruption mitigation system," *Phys. Plasmas* **22**(2), 021802 (2015).
- ⁹M. Lehnen, K. Aleynikova, P. B. Aleynikov, D. J. Campbell, P. Drewelow, N. W. Eidietis, Y. Gasparyan, R. S. Granetz, Y. Gribov, N. Hartmann *et al.*, "Disruptions in ITER and strategies for their control and mitigation," *J. Nucl. Mater.* **463**, 39–48 (2015).
- ¹⁰R. S. Granetz, E. M. Hollmann, D. G. Whyte, V. A. Izzo, G. Y. Antar, A. Bader, M. Bakhtiari, T. Biewer, J. A. Boedo, T. E. Evans *et al.*, "Gas jet disruption mitigation studies on Alcator C-Mod and DIII-D," *Nucl. Fusion* **47**(9), 1086–1091 (2007).
- ¹¹E. M. Hollmann, T. C. Jernigan, P. B. Parks, J. A. Boedo, T. E. Evans, M. Groth, D. A. Humphreys, A. N. James, M. J. Lancot, D. Nishijima *et al.*, "Measurements of injected impurity assimilation during massive gas injection experiments in DIII-D," *Nucl. Fusion* **48**(11), 11507 (2008).
- ¹²C. Reux, J. Bucalossi, F. Saint-Laurent, C. Gil, P. Moreau, and P. Maget, "Experimental study of disruption mitigation using massive injection of noble gases on Tore Supra," *Nucl. Fusion* **50**(9), 095006 (2010).
- ¹³F. Saint-Laurent, C. Reux, J. Bucalossi, A. Loarte, S. Bremond, C. Gil, P. Maget, P. Moreau, and J. L. Segui, "Disruption and runaways electron mitigation studies on Tore Supra," 23rd IAEA Fusion Energy Conf. (Daejeon, Korea Rep. of), EXS 2, 16 (2010); available at https://wwwpub.iaea.org/mtcd/meetings/PDFplus/2010/cn180/cn180_papers/exs_p2-16.pdf
- ¹⁴X. Yang, J. Liu, T. Gao, M. Li, Y. J. Shi, H. F. Liang, W. D. Cai, and Z. Y. Chen, "Magnetic fluctuation level in disruption plasmas in the TEXTOR tokamak," *J. Plasma Phys.* **76**(01), 101–106 (2009).
- ¹⁵M. Gobbin, L. Li, Y. Q. Liu, L. Marrelli, M. Nocente, G. Papp, G. Pautasso, P. Piovesan, M. Valisa, D. Carnevale *et al.*, "Runaway electron mitigation by 3D fields in the ASDEX-Upgrade experiment," *Plasma Phys. Controlled Fusion* **60**(1), 014036 (2018).
- ¹⁶E. M. Hollmann, M. E. Austin, J. A. Boedo, N. H. Brooks, N. Commaux, N. W. Eidietis, D. A. Humphreys, V. A. Izzo, A. N. James, T. C. Jernigan *et al.*, "Control and dissipation of runaway electron beams created during rapid shutdown experiments in DIII-D," *Nucl. Fusion* **53**(8), 083004 (2013).
- ¹⁷C. Reux, V. Plyusnin, B. Alper, D. Alves, B. Bazylev, E. Belonohy, A. Boboc, S. Brezinsek, I. Coffey, J. Decker *et al.*, "Runaway electron beam generation and mitigation during disruptions at JET-ILW," *Nucl. Fusion* **55**(9), 093013 (2015).
- ¹⁸R. Yoshino, S. Tokuda, and Y. Kawano, "Generation and termination of runaway electrons at major disruptions in JT-60U," *J. Nuclear Fusion* **39**(2), 151 (1999).
- ¹⁹S. A. Bozhnikov, M. Lehnen, K. H. Finken, M. W. Jakubowski, R. C. Wolf, R. Jaspers, M. Kantor, O. V. Marchuk, E. Uzel, G. Van Wassenhove *et al.*, "Generation and suppression of runaway electrons in disruption mitigation experiments in TEXTOR," *Plasma Phys. Controlled Fusion* **50**(10), 105007 (2008).
- ²⁰M. Lehnen, S. S. Abdullaev, G. Arnoux, S. A. Bozhnikov, M. W. Jakubowski, R. Jaspers, V. V. Plyusnin, V. Riccardo, and U. Samm, "Runaway generation during disruptions in JET and TEXTOR," *J. Nucl. Mater.* **390–391**, 740–746 (2009).
- ²¹S. S. Abdullaev, K. H. Finken, K. Wongrach, M. Tokar, H. R. Koslowski, O. Willi, and L. Zeng, "Mechanism of runaway electron beam formation during plasma disruptions in tokamaks," *Phys. Plasmas* **22**(4), 040704 (2015).
- ²²L. Zeng, H. R. Koslowski, Y. Liang, A. Lvovskiy, M. Lehnen, D. Nicolai, J. Pearson, M. Rack, H. Jaegers, K. H. Finken *et al.*, "Experimental observation of a magnetic-turbulence threshold for runaway-electron generation in the TEXTOR tokamak," *Phys. Rev. Lett.* **110**(23), 235003 (2013).
- ²³K. H. Finken, S. S. Abdullaev, M. Jakubowski, R. Jaspers, M. Lehnen, and O. Zimmermann, "Losses of runaway electrons during ergodization," *Nucl. Fusion* **46**(4), S139–S44 (2006).
- ²⁴K. H. Finken, S. S. Abdullaev, M. W. Jakubowski, R. Jaspers, M. Lehnen, R. Schlickeiser, K. H. Spatschek, A. Wingen, R. Wolf, and TEXTOR Team, "Runaway losses in ergodized plasmas," *Nucl. Fusion* **47**(2), 91–102 (2007).
- ²⁵M. Lehnen, S. A. Bozhnikov, S. S. Abdullaev, TEXTOR Team, and M. W. Jakubowski, "Suppression of runaway electrons by resonant magnetic perturbations in TEXTOR disruptions," *Phys. Rev. Lett.* **100**(25), 255003 (2008).
- ²⁶R. Yoshino and S. Tokuda, "Runaway electrons in magnetic turbulence and runaway current termination in tokamak discharges," *Nucl. Fusion* **40**(7), 1293 (2000).
- ²⁷N. Commaux, L. R. Baylor, S. K. Combs, N. W. Eidietis, T. E. Evans, C. R. Foust, E. M. Hollmann, D. A. Humphreys, V. A. Izzo, A. N. James *et al.*, "Novel rapid shutdown strategies for runaway electron suppression in DIII-D," *Nucl. Fusion* **51**(10), 103001 (2011).
- ²⁸G. Papp, M. Drevlak, T. Fülöp, P. Helander, and G. I. Pokol, "Runaway electron losses caused by resonant magnetic perturbations in ITER," *Plasma Phys. Controlled Fusion* **53**(9), 095004 (2011).
- ²⁹G. Papp, M. Drevlak, T. Fülöp, and G. I. Pokol, "The effect of resonant magnetic perturbations on runaway electron transport in ITER," *Plasma Phys. Controlled Fusion* **54**(12), 125008 (2012).
- ³⁰Z. Y. Chen, D. W. Huang, V. A. Izzo, R. H. Tong, Z. H. Jiang, Q. M. Hu, Y. N. Wei, W. Yan, B. Rao, S. Y. Wang *et al.*, "Enhancement of runaway production by resonant magnetic perturbation on J-TEXT," *Nucl. Fusion* **56**(7), 074001 (2016).
- ³¹Z. Y. Chen, Z. F. Lin, D. W. Huang, R. H. Tong, Q. M. Hu, Y. N. Wei, W. Yan, A. J. Dai, X. Q. Zhang, B. Rao *et al.*, "Suppression of runaway electrons by mode locking during disruptions on J-TEXT," *Nucl. Fusion* **58**(8), 082002 (2018).
- ³²Z. F. Lin, Z. Y. Chen, D. W. Huang, J. Huang, R. H. Tong, Y. N. Wei, W. Yan, D. Li, Q. M. Hu, Y. Huang *et al.*, "Full suppression of runaway electron generation by the mode penetration of resonant magnetic perturbations during disruptions on J-TEXT," *Plasma Phys. Controlled Fusion* **61**(2), 024005 (2019).
- ³³A. Matsuyama, M. Yagi, Y. Kagei, and N. Nakajima, "Drift resonance effect on stochastic runaway electron orbit in the presence of low-order magnetic perturbations," *Nucl. Fusion* **54**(12), 123007 (2014).
- ³⁴G. Papp, M. Drevlak, T. Fülöp, and P. Helander, "Runaway electron drift orbits in magnetostatic perturbed fields," *Nucl. Fusion* **51**(4), 043004 (2011).
- ³⁵A. H. BOOZER, "Runaway electrons and magnetic island confinement," *Phys. Plasmas* **23**(8), 082514 (2016).
- ³⁶A. H. Boozer, "Magnetic surface loss and electron runaway," *Plasma Phys. Controlled Fusion* **61**(2), 024002 (2019).
- ³⁷A. H. Boozer and A. Punjabi, "Loss of relativistic electrons when magnetic surfaces are broken," *Phys. Plasmas* **23**(10), 102513 (2016).
- ³⁸S. Li, L. Wang, Z. Y. Chen, D. W. Huang, W. Guo, R. H. Tong, and F. T. Cui, "A study on combined effects of stochastic magnetic fluctuations and synchrotron radiation on the production of runaway electrons," *Plasma Phys. Controlled Fusion* **59**(5), 055003 (2017).
- ³⁹J. R. Martín-Solís, A. Loarte, and M. Lehnen, "On the avalanche generation of runaway electrons during tokamak disruptions," *Phys. Plasmas* **22**(8), 082503 (2015).
- ⁴⁰J. R. Martín-Solís, A. Loarte, and M. Lehnen, "Formation and termination of runaway beams in ITER disruptions," *Nucl. Fusion* **57**(6), 066025 (2017).
- ⁴¹S. S. Abdullaev, A. Wingen, and K. H. Spatschek, "Mapping of drift surfaces in toroidal systems with chaotic magnetic fields," *Phys. Plasmas* **13**(4), 042509 (2006).

- ⁴²Z. H. Jiang, X. H. Wang, Z. Y. Chen, D. W. Huang, X. F. Sun, T. Xu, and G. Zhuang, "Simulation of runaway electrons, transport affected by J-TEXT resonant magnetic perturbation," *Nucl. Fusion* **56**(9), 092012 (2016).
- ⁴³A. Wingen, S. S. Abdullaev, K. H. Finken, M. Jakubowski, and K. H. Spatschek, "Influence of stochastic magnetic fields on relativistic electrons," *Nucl. Fusion* **46**(11), 941–952 (2006).
- ⁴⁴E. Nardon, A. Fil, M. Hoelzl, and G. Huijsmans, "Progress in understanding disruptions triggered by massive gas injection via 3D non-linear MHD modelling with JOREK," *Plasma Phys. Controlled Fusion* **59**(1), 014006 (2017).
- ⁴⁵C. Sommariva, E. Nardon, P. Beyer, M. Hoelzl, and G. T. A. Huijsmans, "Electron acceleration in a JET disruption simulation," *Nucl. Fusion* **58**(10), 106022 (2018).
- ⁴⁶C. Sommariva, E. Nardon, P. Beyer, M. Hoelzl, G. T. A. Huijsmans, and D. Van Vugt, "Test particles dynamics in the JOREK 3D non-linear MHD code and application to electron transport in a disruption simulation," *Nucl. Fusion* **58**(1), 016043 (2018).
- ⁴⁷V. A. Izzo, E. M. Hollmann, A. N. James, J. H. Yu, D. A. Humphreys, L. L. Lao, P. B. Parks, P. E. Sieck, J. C. Wesley, R. S. Granetz *et al.*, "Runaway electron confinement modelling for rapid shutdown scenarios in DIII-D, Alcator C-Mod and ITER," *Nucl. Fusion* **51**(6), 063032 (2011).
- ⁴⁸V. A. Izzo, D. A. Humphreys, and M. Kornbluth, "Analysis of shot-to-shot variability in post-disruption runaway electron currents for diverted DIII-D discharges," *Plasma Phys. Controlled Fusion* **54**(9), 095002 (2012).
- ⁴⁹V. A. Izzo, "The effect of pre-existing islands on disruption mitigation in MHD simulations of DIII-D," *Phys. Plasmas* **24**(5), 056102 (2017).
- ⁵⁰V. A. Izzo, D. G. Whyte, R. S. Granetz, P. B. Parks, E. M. Hollmann, L. L. Lao, and J. C. Wesley, "Magnetohydrodynamic simulations of massive gas injection into Alcator C-Mod and DIII-D plasmas," *Phys. Plasmas* **15**(5), 056109 (2008).
- ⁵¹V. A. Izzo and I. Joseph, "RMP enhanced transport and rotational screening in simulations of DIII-D plasmas," *Nucl. Fusion* **48**(11), 115004 (2008).
- ⁵²C. R. Sovinec, A. H. Glasser, T. A. Gianakon, D. C. Barnes, R. A. Nebel, S. E. Kruger, D. D. Schnack, S. J. Plimpton, A. Tarditi, and M. S. Chu, "Nonlinear magnetohydrodynamics simulation using high-order finite elements," *J. Comput. Phys.* **195**(1), 355–386 (2004).
- ⁵³B. Rao, G. Wang, Y. H. Ding, K. X. Yu, Q. L. Li, N. C. Wang, B. Yi, J. Y. Nan, Y. S. Cen, Q. M. Hu *et al.*, "Introduction to resonant magnetic perturbation coils of the J-TEXT tokamak," *Fusion Eng. Des.* **89**(4), 378–384 (2014).
- ⁵⁴V. A. Izzo and P. B. Parks, "Comment on: Plasma current spikes due to internal reconnection during tokamak disruptions," *Nucl. Fusion* **50**(5), 058001 (2010).
- ⁵⁵V. A. Izzo, "Impurity mixing and radiation asymmetry in massive gas injection simulations of DIII-D," *Phys. Plasmas* **20**(5), 056107 (2013).
- ⁵⁶A. Fil, E. Nardon, M. Hoelzl, G. T. A. Huijsmans, F. Orain, M. Becoulet, P. Beyer, G. Dif-Pradalier, R. Guirlet, H. R. Koslowski *et al.*, "Three-dimensional non-linear magnetohydrodynamic modeling of massive gas injection triggered disruptions in JET," *Phys. Plasmas* **22**(6), 056107 (2015).
- ⁵⁷V. A. Izzo, "A numerical investigation of the effects of impurity penetration depth on disruption mitigation by massive high-pressure gas jet," *Nucl. Fusion* **46**(5), 541–547 (2006).
- ⁵⁸L. Zeng, Z. Y. Chen, Y. B. Dong, H. R. Koslowski, Y. Liang, Y. P. Zhang, H. D. Zhuang, D. W. Huang, and X. Gao, "Runaway electron generation during disruptions in the J-TEXT tokamak," *Nucl. Fusion* **57**(4), 046001 (2017).
- ⁵⁹T. Fehér, H. M. Smith, T. Fülöp, and K. Gál, "Simulation of runaway electron generation during plasma shutdown by impurity injection in ITER," *Plasma Phys. Controlled Fusion* **53**(3), 035014 (2011).
- ⁶⁰H. M. Smith and E. Verwichte, "Hot tail runaway electron generation in tokamak disruptions," *Phys. Plasmas* **15**(7), 072502 (2008).
- ⁶¹R. H. Tong, Z. F. Lin, L. Z. Liu, W. Li, Y. N. Wei, D. Li, X. M. Pan, P. Shi, N. C. Wang, and Z. Y. Chen, "The effect of $m/n = 2/1$ locked mode on disruption process during massive gas injection shutdown on J-TEXT," *Nucl. Fusion* (to be published).